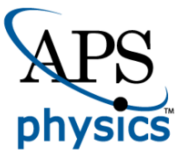

Testing the multipole structure of compact binaries using gravitational wave observations

Shilpa Kastha, Anuradha Gupta, K. G. Arun, B. S. Sathyaprakash, and Chris Van Den Broeck

Phys. Rev. D **98**, 124033 — Published 26 December 2018

DOI: 10.1103/PhysRevD.98.124033

Testing the multipole structure of compact binaries using gravitational wave observations

Shilpa Kastha,[1,*] Anuradha Gupta,[2,†] K. G. Arun,[3,2,‡] B. S. Sathyaprakash,[2,4,5,§] and Chris Van Den Broeck[6,7,¶]

[1]*Institute of Mathematical Sciences, HBNI, CIT Campus, Chennai-600113, India*
[2]*Institute for Gravitation and the Cosmos, Department of Physics, Penn State University, University Park PA 16802, USA*
[3]*Chennai Mathematical Institute, Siruseri, 603103, India*
[4]*Department of Astronomy and Astrophysics, Penn State University, University Park PA 16802, USA*
[5]*School of Physics and Astronomy, Cardiff University, Cardiff, CF24 3AA, United Kingdom*
[6]*Nikhef - National Institute for Subatomic Physics, Science Park 105, 1098 XG Amsterdam, The Netherlands*
[7]*Van Swinderen Institute for Particle Physics and Gravity, University of Groningen, Nijenborgh 4, 9747 AG Groningen, The Netherlands*

We propose a novel method to test the consistency of the multipole moments of compact binary systems with the predictions of General Relativity (GR). The multipole moments of a compact binary system, known in terms of symmetric and trace-free tensors, are used to calculate the gravitational waveforms from compact binaries within the post-Newtonian (PN) formalism. For nonspinning compact binaries, we derive the gravitational wave phasing formula, in the frequency domain, parametrizing each PN order term in terms of the multipole moments which contribute to that order. Using GW observations, this *parametrized multipolar phasing* would allow us to derive the bounds on possible departures from the multipole structure of GR and hence constrain the parameter space of alternative theories of gravity. We compute the projected accuracies with which the second generation ground-based detectors, such as Advanced Laser Interferometer Gravitational-wave Observatory (LIGO), the third generation detectors such as Einstein Telescope and Cosmic Explorer, as well as space-based detector Laser Interferometer Space Antenna (LISA) will be able to measure these multipole parameters. We find that while Advanced LIGO can measure the first two or three multipole coefficients with good accuracy, Cosmic Explorer and Einstein Telescope may be able to measure the first four multipole coefficients which enter the phasing formula. Intermediate mass ratio inspirals, with mass ratio of several tens, in the frequency band of planned space-based LISA mission should be able to measure all the seven multipole coefficients which appear in the 3.5PN phasing formula. Our finding highlights the importance of this class of sources for probing the strong-field gravity regime. The proposed test will facilitate the first probe of the multipolar structure of Einstein's general relativity.

I. INTRODUCTION

The discovery of binary black holes [1–4] and binary neutron stars [5] by Advanced LIGO [6] and Advanced Virgo [7] have been ground breaking for several reasons. Among the most important aspects of these discoveries is the unprecedented opportunity they have provided to study the behavior of gravity in the highly nonlinear and dynamical regime associated with the merger of two black holes (BHs) or two neutron stars (see Refs. [8, 9] for reviews). The gravitational wave (GW) observations have put stringent constraints on the allowed parameter space of alternative theories of gravity by different methods [3, 10, 11]. They include the parametrized tests of post-Newtonian theory [12–18], bounding the mass of the putative graviton and dispersion of GWs [19, 20], testing consistency between the inspiral and ringdown regimes of the coalescence [21] and the time delay between the GW and electromagnetic signals [22]. Furthermore, the bounds obtained from these tests have been translated into bounds on the free parameters of certain specific theories of gravity [23].

With improved sensitivities of Advanced LIGO and Virgo in the upcoming observing runs, the development of third generation detectors such as the Einstein Telescope (ET) [24] and Cosmic Explorer (CE) [25] and the approval of funding for the space-based mission LISA [26], the field of gravitational astronomy promises to deliver exciting science returns. In addition to stellar-mass compact binaries, future ground-based detectors, such as ET and CE, can detect intermediate mass black holes with a total mass of several hundreds of solar mass. Such observations will not only confirm the existence of BHs in this mass range (see [27, 28] for reviews), but also facilitate several new probes of fundamental physics via studying their dynamics [29–32]. One of the most prominent, among these, are those using intermediate mass ratio inspirals, which will last longer (compared to the equal mass binaries), and hence an accurate probe of the compact binary dynamics and the BH nature of the central compact object [31, 33].

Space-based LISA mission, on the other hand, will be sensitive to milli-Hertz GWs produced by the inspiral and merger of supermassive BH binaries in the mass range $\sim 10^4$-$10^7 M_\odot$. These sources may also have a large diversity in the mass ratios ranging from comparable mass (mass ratio $\lesssim 10$) and intermediate mass ratios (mass ratio $\gtrsim 100$) to extreme mass ratios (mass ratio $\gtrsim 10^6$) where a stellar mass BH spirals into the central supermassive BH with several millions of solar masses [34, 35]. This diversity together with the sensitivity in the low frequency window makes LISA a very efficient probe of possible deviations from GR in different regimes of dynamics (see [8, 36–38] for reviews).

* shilpakastha@imsc.res.in
† axg645@psu.edu
‡ kgarun@cmi.ac.in
§ bss25@psu.edu
¶ vdbroeck@nikhef.nl

Setting stringent limits on possible departures from GR as well as constraining the parameter space of exotic compact objects that can mimic the properties of BH [39–46], are among the principle science goals of the next generation detectors. They should also be able to detect any new physics, or modification to GR, if present.

Formulating new methods to carry out such tests is crucial in order to efficiently extract the physics from GW observations. Dynamics of a compact binary system is conventionally divided to *adiabatic inspiral, rapid merger* and fast ringdown. During the inspiral phase the orbital time scale is much smaller than the radiation back-reaction time scale. Post-Newtonian (PN) approximation to GR has proved to be a very effective method to describe the inspiral phase of a compact binary of comparable masses [47]. Description of the highly nonlinear phase of the merger of two compact objects needs numerical solutions to the Einstein's equations [48]. The ringdown radiation of GWs by the merger remnant, can be modelled within the framework of BH perturbation theory [49]. In alternative theories of gravity, the dynamics of the compact binary during these phases of evolution could be quite different from that predicted by GR. Hence observing GWs is the best way to probe the presence of non-GR physics associated with the phenomenon.

One of the most generic tests of the binary dynamics has been the measurement of the PN coefficients of the GW phasing formula [12–16, 50, 51]. This test captures a possible departure from GR by measuring the PN coefficients in the phase evolution of the GW signal. In addition to the source physics, the different PN terms in the phase evolution contain information about different nonlinear interaction the wave undergoes as it propagates from the source to the detector. Hence the predictions for these effects in an alternative theory of gravity could be very different from that of GR, which is what is being tested using the parametrized tests of PN theory.

In this work, we go one step further and propose a novel way to test the multipolar structure of the gravitational field of a compact binary as it evolves through the adiabatic inspiral phase. The multipole moments of the compact binary (and interactions between them), are responsible for the various physical effects we see at different PN orders. By measuring these effects we can constrain the multipolar structure of the system. The GW phase and frequency evolution is obtained from the energy flux of GWs and the conserved orbital energy by using the energy balance argument, which equates the GW energy flux $\mathcal{F}$ to the decrease in the binding energy $E_{\rm orb}$ of the binary [52]

$$\mathcal{F} = -\frac{d}{dt}E_{\rm orb}. \tag{1.1}$$

In an alternative theory of gravity, one or more multipole moments of a binary system may be different from those of GR. For instance, in Ref. [53], the authors discuss how effective field theory-based approach can be used to go beyond Einstein's gravity by introducing additional terms to the GR Lagrangian which are higher order operators constructed out of Riemann tensor, but suppressed by appropriate scales comparable to curvature of the compact binaries. They find that such generic modifications will lead to multipole moments of compact binaries that are different from GR. Our proposed method aims to constrain such generic extensions of GR by directly measuring multipole moments of the compact binaries through GW observations.

In this work, we assume that the conserved orbital energy of the binary is the same as in GR and modify the gravitational wave flux by deforming the multipole moments which contribute to it by employing the multipolar post-Minkowskian formalism [47, 52]. We then re-derive the GW phase and its frequency evolution (sometimes referred to as the phasing formula) explicitly in terms of the various deformed multipole moments (In the appendix we provide a more general expression for the phasing where the conserved energy is also deformed at different PN orders, in addition to the multipole moments of the source.). We use this parameterized multipolar phasing formula to measure possible deviations from GR and discuss the level of bounds we can expect from the current and next generation ground-based GW detectors, as well as the space-based LISA detector. We obtain measurement accuracy of the system's physical parameters and the deformation of the multipole moments using the semi-analytical Fisher information matrix [54, 55]. These results are validated for several configurations of the binary system by Markov Chain Monte Carlo (MCMC) sampling of the likelihood function using `emcee` [56] algorithm.

We find that Advanced LIGO-like detectors can constrain at most two of the leading multipoles, while a third generation detector, such as ET or CE, can set constraints on as many as four of the leading multipoles. The space-based LISA detector will have the ability to set good limits on all the seven multipole moments that contribute to the 3.5PN phasing formula, making it a very accurate probe of the highly nonlinear dynamics of compact binaries.

The organization of the paper is as follows. In Sec. II we describe the basic formalism to obtain the parametrized multipolar GW phasing formula. In Sec. III we briefly explain the two parameter estimation schemes (Fisher information matrix and Bayesian inference) used in our analysis, followed by Sec. IV where we discuss the results we obtained for various ground-based and space-based detectors. Section V summarizes the paper and lists some of the follow-ups we are pursuing.

II. PARAMETRIZED MULTIPOLAR GRAVITATIONAL WAVE PHASING

The two-body problem in GR can be solved perturbatively using PN theory in the adiabatic regime, where the orbital time scale is much smaller than the radiation back-reaction time scale (see Ref. [47] for a review). The PN theory has given us several useful insights about various facets of the two-body dynamics and the resulting gravitational radiation.

In the Multipolar post-Minkowskian (MPM) formalism [52, 57–67], the important quantities such as the gravitational waveform, energy and angular momentum fluxes can be expressed using a combination of post-Minkowskian approximation (expansion in powers of G, the Newton's gravitational constant,

valid throughout the spacetime for weakly gravitating sources), PN expansions (an expansion in $1/c$ that is valid for slowly moving and weakly gravitating sources and applicable in the near zone of the source) and multipole expansion of the gravitational field valid all over the region exterior to the source. Coefficients of post-Minkowskian expansion and the multipole moments of the source can be further expanded as a PN series. Multipole expansion of the gravitational field plays a central role in the analytical treatment of the two-body problem as it significantly helps to handle the nonlinearities of Einstein's equations.

The MPM formalism relates the radiation content in the far-zone (at the detector) to the stress-energy tensor of the source. The quantities in the far-zone are described by mass- and current-type *radiative* multipole moments $\{U_L, V_L\}$ whereas the properties of the source are completely described by the mass- and current-type source multipole moments $\{I_L, J_L\}$ and the four gauge moments $\{W_L, X_L, Y_L, Z_L\}$ all of which are the moments of the relativistic mass and current densities expressed as functionals of the stress-energy pseudo-tensor of the source and gravitational fields. However, in GR, there is further gauge freedom to reduce this set of six source moments to a set of two "canonical" multipole moments $\{M_L, S_L\}$. The relations connecting these two sets of multipole moments can be found in Eqs. (97) and (98) of [47]. Furthermore, the mass- and current-type radiative multipole moments $\{U_L, V_L\}$ admit closed-form expressions in terms of $\{M_L, S_L\}$.

The source and the canonical multipole moments are usually expressed using the basis of symmetric trace-free tensors [68]. The relationships between the radiative and the source type multipole moments incorporate the various non-linear interactions between the various multipoles, such as tails [52, 69, 70], tails-of tails [71], tail-square [72], memory [73–76], . . . , as the wave propagates from the source to the detector (see ref. [47] for more details).

For quasi-circular inspiral, the PN expressions for orbital energy and the energy flux, together with the energy balance argument is used in the computation of the GW phasing formula at any PN order [52, 67, 77, 78]. The PN terms in the phasing formula, hence, explicitly encode the information about the multipolar structure of the gravitational field of the two-body dynamics.

In this work, we separately keep track of the contributions from various radiative multipole moments to the GW flux allowing us to derive a parametrized multipolar gravitational-wave flux and phasing formula, thereby permitting tests of multipolar structure of the PN approximation to GR. We first re-derive the phasing formula for non-spinning compact binaries moving in quasi-circular orbits up to 3.5 PN order. The computation is detailed in the next section. Before we proceed, we clarify that in our notation first post-Newtonian (1PN) correction would refer to corrections of order v^2/c^2, where $v = (\pi m f)^{1/3}$ is the characteristic orbital velocity of the binary, m is the total mass of the binary and f is the orbital frequency.

A. The multipolar structure of the energy flux

The multipole expansion of the energy flux within the MPM formalism schematically reads as [52, 57]

$$\mathcal{F} = \sum_l \left[\frac{\alpha_l}{c^{l-2}} U_L^{(1)} U_L^{(1)} + \frac{\beta_l}{c^l} V_L^{(1)} V_L^{(1)} \right], \tag{2.1}$$

where α_l, β_l are known real numbers and U_L, V_L are mass- and current-type radiative multipole moments with l indices; the superscript (1) denotes the first time-derivative of the multipoles. The U_L and V_L can be re-written in terms of the source multipole moments as

$$U_L = M_L^{(l)} + \text{Nonlinear interaction terms}, \tag{2.2}$$

$$V_L = S_L^{(l)} + \text{Nonlinear interaction terms}, \tag{2.3}$$

where the right hand side involves l^{th} time-derivative of the mass- and current-type source multipole moments and nonlinear interactions between the various multipoles due to the propagation of the wave in the curved spacetime of the source. (see [63, 65, 71, 72] for details.) The various types of interactions can be decomposed as follows [52, 65]

$$\mathcal{F} = \mathcal{F}_{\text{inst}} + \mathcal{F}_{\text{tail}} + \mathcal{F}_{\text{tail}^2} + \mathcal{F}_{\text{tail(tail)}}. \tag{2.4}$$

As opposed to the $\mathcal{F}_{\text{inst}}$ (a contribution that depends on the dynamics of the binary at the purely retarded instant of time, referred to as instantaneous terms), the last three contributions $\mathcal{F}_{\text{tail}}$, $\mathcal{F}_{\text{tail}^2}$ and $\mathcal{F}_{\text{tail(tail)}}$ contain nonlinear multipolar interactions in the flux [71] that depend on the dynamical history of the system, referred to as *hereditary* contribution.

In an alternative theory of gravity, the multipole moments may not be the same as in GR; if the mass- and current-type radiative multipole moments deviate from their GR value by a fractional amount δU_L and δV_L, i.e., $U_L \to U_L^{\text{GR}} + \delta U_L$ and $V_L \to V_L^{\text{GR}} + \delta V_L$, then we can parametrize such deviations in the multipoles by considering the scalings

$$\begin{aligned} U_L &\to \mu_l \, U_L, \\ V_L &\to \epsilon_l \, V_L, \end{aligned} \tag{2.5}$$

where the parameters $\mu_l = 1 + \delta U_L / U_L^{\text{GR}}$ and $\epsilon_l = 1 + \delta V_L / V_L^{\text{GR}}$ are equal to unity in GR.

We first recompute the GW flux from non-spinning binaries moving in quasi-circular orbit up to 3.5PN order with the above scaling using the prescription outlined in [52, 64, 65, 67]. With the parameterizations introduced above, the computation of the energy flux would proceed similar to that in GR but contribution from every radiative multipole is now separately kept track of.

In order to calculate the fluxes up to the required PN order, we need to compute the time derivatives of the multipole moments as can be seen from Eqs. (2.1)-(2.3). These are computed by using the equations of motion of the compact binary for quasi-circular orbits given by [65, 79]

$$\frac{d\mathbf{v}}{dt} = -\omega^2 \, \mathbf{x}, \tag{2.6}$$

where the expression for ω, the angular frequency of the binary, up to 3PN order is given by [66, 78–83]

$$\omega^2 = \frac{Gm}{r^3}\Bigg\{1 + [-3+\nu]\,\gamma + \left[6 + \frac{41}{4}\nu + \nu^2\right]\gamma^2 + \left[-10 + \left(22\ln\left(\frac{r}{r'_0}\right) + \frac{41\pi^2}{64} - \frac{75707}{840}\right)\nu + \frac{19}{2}\nu^2 + \nu^3\right]\gamma^3 + O(\gamma^4)\Bigg\}, \tag{2.7}$$

where $\gamma = Gm/rc^2$ is a PN parameter, r'_0 is a gauge dependent length scale which does not appear when observables, such as the energy flux, are expressed in terms of gauge independent variables.

The hereditary terms are calculated using the prescriptions given in Refs. [52, 65, 70, 84] for tails, Ref. [71] for tails of tails and Ref. [72] for tail-square. The complete expression for the energy flux $\mathcal{F}$ in terms of the scaled multipoles is given as

$$\begin{aligned}
\mathcal{F} =& \frac{32}{5}\frac{c^5 v^{10}}{G}\nu^2\mu_2^2\Bigg\{1 + v^2\left(-\frac{107}{21} + \frac{55}{21}\nu + \hat{\mu}_3^2\left[\frac{1367}{1008} - \frac{1367}{252}\nu\right] + \hat{\epsilon}_2{}^2\left[\frac{1}{36} - \frac{\nu}{9}\right]\right) + 4\pi v^3 + v^4\left(\frac{4784}{1323} - \frac{87691}{5292}\nu\right.\\
&+\frac{5851}{1323}\nu^2 + \hat{\mu}_3^2\left[-\frac{32807}{3024} + \frac{3515}{72}\nu - \frac{8201}{378}\nu^2\right] + \hat{\mu}_4^2\left[\frac{8965}{3969} - \frac{17930}{1323}\nu + \frac{8965}{441}\nu^2\right] + \hat{\epsilon}_2{}^2\left[-\frac{17}{504} + \frac{11}{63}\nu - \frac{10}{63}\nu^2\right]\\
&\left.+\hat{\epsilon}_3{}^2\left[\frac{5}{63} - \frac{10}{21}\nu + \frac{5}{7}\nu^2\right]\right) + \pi v^5\left(-\frac{428}{21} + \frac{178}{21}\nu + \hat{\mu}_3^2\left[\frac{16403}{2016} - \frac{16403}{504}\nu\right] + \hat{\epsilon}_2{}^2\left[\frac{1}{18} - \frac{2}{9}\nu\right]\right)\\
&+v^6\left(\frac{99210071}{1091475} + \frac{16\pi^2}{3} - \frac{1712}{105}\gamma - \frac{856}{105}\log[16v^2] + \left[\frac{1650941}{349272} + \frac{41\pi^2}{48}\right]\nu - \frac{669017}{19404}\nu^2 + \frac{255110}{43659}\nu^3\right.\\
&+\hat{\mu}_3^2\left[\frac{7345}{297} - \frac{30103159}{199584}\nu + \frac{10994153}{49896}\nu^2 - \frac{45311}{891}\nu^3\right] + \hat{\mu}_4^2\left[-\frac{1063093}{43659} + \frac{20977942}{130977}\nu - \frac{12978200}{43659}\nu^2\right.\\
&\left.+\frac{1568095}{14553}\nu^3\right] + \hat{\mu}_5^2\left[\frac{1002569}{249480} - \frac{1002569}{31185}\nu + \frac{1002569}{12474}\nu^2 - \frac{2005138}{31185}\nu^3\right] + \hat{\epsilon}_2^2\left[-\frac{2215}{254016} - \frac{13567}{63504}\nu + \frac{65687}{63504}\nu^2\right.\\
&\left.-\frac{853\nu^3}{5292}\right] + \hat{\epsilon}_3{}^2\left[-\frac{193}{567} + \frac{1304}{567}\nu - \frac{2540}{567}\nu^2 + \frac{365}{189}\nu^3\right] + \hat{\epsilon}_4{}^2\left[\frac{5741}{35280} - \frac{5741}{4410}\nu + \frac{5741}{1764}\nu^2 - \frac{5741}{2205}\nu^3\right]\Bigg)\\
&+\pi v^7\left(\frac{19136}{1323} - \frac{144449}{2646}\nu + \frac{33389}{2646}\nu^2 + \hat{\mu}_3^2\left[-\frac{98417}{1512} + \frac{55457}{192}\nu - \frac{344447}{3024}\nu^2\right] + \hat{\mu}_4^2\left[\frac{23900}{1323} - \frac{47800}{441}\nu\right.\right.\\
&\left.\left.+\frac{23900}{147}\nu^2\right] + \hat{\epsilon}_2{}^2\left[-\frac{17}{252} + \frac{9}{28}\nu - \frac{13}{63}\nu^2\right] + \hat{\epsilon}_3{}^2\left[\frac{20}{63} - \frac{40}{21}\nu + \frac{20}{7}\nu^2\right]\right)\Bigg\},
\end{aligned} \tag{2.8}$$

where $\hat{\mu}_\ell = \mu_\ell/\mu_2$, $\hat{\epsilon}_\ell = \epsilon_\ell/\mu_2$, ν is the symmetric mass ratio defined as the ratio of reduced mass μ to the total mass m. As an algebraic check of the result, we recover the GR results of [65] in the limit $\mu_l \to 1, \epsilon_l \to 1$.

B. Conservative Dynamics of the binary

A model for the conservative dynamics of the binary is also required to compute the phase evolution of the system. This enters the phasing formula in two ways. Firstly, the equation of motion of the binary [79] in the center-of-mass frame is required to compute the derivatives of the multipole moments while calculating the energy flux. Secondly, the expression for the 3PN orbital energy [78, 79] is necessary to compute the equation of energy balance to obtain the phase evolution (see Eqs. (2.13)–(2.14) below). As the computation of the radiative multipole moments require two or more derivative operations, they are implicitly sensitive to the equation of motion. Hence, formally, a constraint on the deformation of the radiative multipole moment does take into account a potential deviation in the equation of motion from the predictions of GR.

Here however we assume the conserved energy to be the same as in GR. This assumption is motivated by practical considerations. We could have taken a more generic approach by deforming the PN coefficients in the equation of motion and conserved energy as well. As the former is degenerate with the definition of radiative multipole moments, one would need to consider a parametrized expression for conserved energy which will give us a phasing formula with four additional parameters corresponding to the different PN orders in the expression for conserved energy. Simultaneous estimation of these parameters with the multipole coefficients would significantly degrade the resulting bounds and may not yield meaningful constraints. However, in the appendix, we present a parametrized phasing formula where in addition to the multipole coefficients, various PN order terms in the conserved 3PN energy expression is also deformed (see Eq. (A.2) below). Interestingly, as can be seen from Eq. (A.2), if there is a modification to the conservative dynamics, they will be fully degenerate with at least one of the multipole coefficients appearing at the same order. Due to this

degeneracy, such modifications will be detected by this test as modifications to "effective" multipole moments. Further, this degeneracy is not accidental. It can be shown that by differentiating the expression for conserved energy, one can derive the energy flux by systematically accounting for the equation of motion, including radiation reaction terms [85, 86]. We are, therefore, confident that the power of the proposed test is not diminished by this assumption. The conserved energy (per unit mass) up to 3PN order is given by [66, 78–83]

$$E(v) = -\frac{1}{2}\nu v^2\left[1-\left(\frac{3}{4}+\frac{1}{12}\nu\right)v^2-\left(\frac{27}{8}-\frac{19}{8}\nu+\frac{1}{24}\nu^2\right)v^4 -\left\{\frac{675}{64}-\left(\frac{34445}{576}-\frac{205}{96}\pi^2\right)\nu+\frac{155}{96}\nu^2 +\frac{35}{5184}\nu^3\right\}v^6\right]. \tag{2.9}$$

Using the expressions for the modified flux and the orbital energy we next proceed to compute the phase evolution of the compact binary.

C. Computation of the parametrized multipolar phasing formula

With the parametrized multipolar flux and the energy expressions, we compute the 3.5PN, nonspinning, frequency-domain phasing formula following the standard prescription [87, 88] by employing the stationary phase approximation (SPA) [89]. Consider a GW signal of the form

$$h(t) = \mathcal{A}(t)\cos\phi(t). \tag{2.10}$$

The Fourier transform of the signal will involve an integrand whose amplitude is slowly varying and phase is rapidly oscillating. In the SPA, dominant contributions to this integral comes from the vicinity of the stationary points of its phase [87]. As a result the frequency domain gravitational waveform may be expressed as

$$\tilde{h}^{\rm SPA}(f) = \frac{\mathcal{A}(t_f)}{\sqrt{\dot{F}(t_f)}}e^{i[\psi_f(t_f)-\pi/4]}, \tag{2.11}$$

$$\psi_f(t) = 2\pi f t - \phi(t), \tag{2.12}$$

where t_f can be obtained by solving $d\psi_f(t)/dt\big|_{t_f} = 0$, $F(t)$ is the gravitational-wave frequency and at $t = t_f$ the GW frequency coincides with the Fourier variable f. More explicitly,

$$t_f = t_{\rm ref} + m\int_{v_f}^{v_{ref}}\frac{E'(v)}{\mathcal{F}(v)}dv, \tag{2.13}$$

$$\psi_f(t_f) = 2\pi f t_{\rm ref} - \phi_{\rm ref} + 2\int_{v_f}^{v_{ref}}(v_f^3 - v^3)\frac{E'(v)}{\mathcal{F}(v)}dv, \tag{2.14}$$

where $E'(v)$ is the derivative of the binding energy of the system expressed in terms of the PN expansion parameter v. Expanding the factor in the integrand in Eq. (2.14) as a PN series and truncating upto 3.5PN order, we obtain the 3.5PN accurate TaylorF2 phasing formula.

We follow the very same procedure, except we use Eq. (2.8) to be the parametrized flux, $\mathcal{F}$, and together with the leading quadrupolar order amplitude (related to the Newtonian GW polarizations), we derive the standard *restricted* PN waveform in frequency domain, which reads as

$$\tilde{h}(f) = \mathcal{A}\mu_2 f^{-7/6}e^{i\psi(f)}, \tag{2.15}$$

with $\psi(f)$ being the parametrized multipolar phasing, $\mathcal{A} = \mathcal{M}_c^{5/6}/\sqrt{30}\pi^{2/3}D_L$; $\mathcal{M}_c = (m_1m_2)^{3/5}/(m_1+m_2)^{1/5}$ and D_L being the chirp mass and luminosity distance, respectively, and m_1, m_2 denote the component masses of the binary. Note the presence of μ_2 in the GW amplitude, this is due to the mass quadrupole that contributes to the amplitude at the leading PN order. If we incorporate the higher order PN terms in the GW polarizations [75, 90, 91], higher order multipoles will enter the GW amplitude as well.

Finally the expression for 3.5PN frequency domain phasing $\psi(f)$ is given by,

$$\psi(f) = 2\pi f t_c - \frac{\pi}{4} - \phi_c + \frac{3}{128v^5\mu_2^2\nu}\Bigg\{1 + v^2\left(\frac{1510}{189}-\frac{130}{21}\nu+\hat{\mu}_3^2\left[-\frac{6835}{2268}+\frac{6835}{567}\nu\right]+\hat{\epsilon}_2{}^2\left[-\frac{5}{81}+\frac{20}{81}\nu\right]\right) -16\pi v^3 + v^4\left(\frac{242245}{5292}+\frac{4525}{5292}\nu+\frac{145445}{5292}\nu^2+\hat{\mu}_3^2\left[-\frac{66095}{7056}+\frac{170935}{3024}\nu-\frac{403405}{5292}\nu^2\right]+\hat{\mu}_3^2\hat{\epsilon}_2{}^2\left[\frac{6835}{9072} -\frac{6835}{1134}\nu+\frac{6835\nu^2}{567}\right]+\hat{\mu}_3^4\left[\frac{9343445}{508032}-\frac{9343445}{63504}\nu+\frac{9343445}{31752}\nu^2\right]+\hat{\mu}_4^2\left[-\frac{89650}{3969}+\frac{179300}{1323}\nu-\frac{89650}{441}\nu^2\right] +\hat{\epsilon}_2{}^2\left[-\frac{785}{378}+\frac{7115}{756}\nu-\frac{835}{189}\nu^2\right]+\hat{\epsilon}_2{}^4\left[\frac{5}{648}-\frac{5}{81}\nu+\frac{10}{81}\nu^2\right]+\hat{\epsilon}_3{}^2\left[-\frac{50}{63}+\frac{100}{21}\nu-\frac{50}{7}\nu^2\right]\right) +\pi v^5\left(3\log\left[\frac{v}{v_{\rm LSO}}\right]+1\right)\left(\frac{80}{189}\left[151-138\nu\right]-\frac{9115}{756}\hat{\mu}_3^2\left[1-4\nu\right]-\frac{20}{27}\hat{\epsilon}_2{}^2\left[1-4\nu\right]\right)+v^6\left(\frac{5334452639}{2037420} -\frac{640}{3}\pi^2-\frac{6848}{21}\gamma-\frac{6848}{21}\log[4v]-\left[\frac{7153041685}{1222452}-\frac{2255}{12}\pi^2\right]\nu+\frac{123839990}{305613}\nu^2+\frac{18300845}{1222452}\nu^3$$

$$+\hat{\mu}_3^2\Bigg[-\frac{4809714655}{29338848}+\frac{8024601785}{9779616}\nu-\frac{19149203695}{29338848}\nu^2-\frac{190583245}{7334712}\nu^3\Bigg]+\hat{\mu}_3^2\hat{\epsilon}_2{}^2\Bigg[-\frac{656195}{95256}+\frac{229475\nu}{3888}$$
$$-\frac{3369935\nu^2}{23814}+\frac{82795\nu^3}{1323}\Bigg]+\hat{\mu}_3^2\hat{\epsilon}_2{}^4\Bigg[\frac{6835}{108864}-\frac{6835}{9072}\nu+\frac{6835}{2268}\nu^2-\frac{6835}{1701}\nu^3\Bigg]+\hat{\mu}_3^2\hat{\epsilon}_3{}^2\Bigg[-\frac{34175}{7938}+\frac{170875}{3969}\nu$$
$$-\frac{375925}{2646}\nu^2+\frac{68350}{441}\nu^3\Bigg]+\hat{\mu}_3^2\hat{\mu}_4^2\Bigg[-\frac{61275775}{500094}+\frac{306378875}{250047}\nu-\frac{674033525}{166698}\nu^2+\frac{122551550}{27783}\nu^3\Bigg]$$
$$+\hat{\mu}_3^4\Bigg[\frac{868749005}{10668672}-\frac{2313421945}{3556224}\nu+\frac{191974645}{148176}\nu^2+\frac{9726205}{666792}\nu^3\Bigg]+\hat{\mu}_3^4\hat{\epsilon}_2{}^2\Bigg[\frac{9343445}{3048192}-\frac{9343445}{254016}\nu$$
$$+\frac{9343445}{63504}\nu^2-\frac{9343445}{47628}\nu^3\Bigg]+\hat{\mu}_3^6\Bigg[\frac{12772489315}{256048128}-\frac{12772489315}{21337344}\nu+\frac{12772489315}{5334336}\nu^2-\frac{12772489315}{4000752}\nu^3\Bigg]$$
$$+\hat{\mu}_4^2\Bigg[-\frac{86554310}{916839}+\frac{553387330}{916839}\nu-\frac{289401650}{305613}\nu^2-\frac{4322750}{101871}\nu^3\Bigg]+\hat{\mu}_4^2\hat{\epsilon}_2{}^2\Bigg[-\frac{89650}{35721}+\frac{896500}{35721}\nu$$
$$-\frac{986150}{11907}\nu^2+\frac{358600\nu^3}{3969}\Bigg]+\hat{\mu}_5^2\Bigg[\frac{1002569}{12474}-\frac{4010276}{6237}\nu+\frac{10025690}{6237}\nu^2-\frac{8020552}{6237}\nu^3\Bigg]$$
$$+\hat{\epsilon}_2{}^2\Bigg[\frac{3638245}{190512}-\frac{2842015}{31752}\nu+\frac{760985}{13608}\nu^2-\frac{328675}{23814}\nu^3\Bigg]+\hat{\epsilon}_2{}^2\hat{\epsilon}_3{}^2\Bigg[-\frac{50}{567}+\frac{500}{567}\nu-\frac{550}{189}\nu^2+\frac{200}{63}\nu^3\Bigg]$$
$$+\hat{\epsilon}_2{}^4\Bigg[-\frac{265}{1512}+\frac{20165}{13608}\nu-\frac{5855}{1701}\nu^2+\frac{310}{243}\nu^3\Bigg]+\hat{\epsilon}_2{}^6\Bigg[\frac{5}{11664}-\frac{5}{972}\nu+\frac{5}{243}\nu^2-\frac{20}{729}\nu^3\Bigg]$$
$$+\hat{\epsilon}_3{}^2\Bigg[\frac{27730}{3969}-\frac{179990}{3969}\nu+\frac{341450}{3969}\nu^2-\frac{51050}{1323}\nu^3\Bigg]+\hat{\epsilon}_4{}^2\Bigg[\frac{5741}{1764}-\frac{11482}{441}\nu+\frac{28705}{441}\nu^2-\frac{22964}{441}\nu^3\Bigg]\Bigg)$$
$$+\pi v^7\Bigg(\frac{484490}{1323}-\frac{141520}{1323}\nu+\frac{442720}{1323}\nu^2+\hat{\mu}_3^2\Bigg[-\frac{88205}{2352}+\frac{63865}{252}\nu-\frac{182440}{441}\nu^2\Bigg]+\hat{\mu}_3^2\hat{\epsilon}_2{}^2\Bigg[\frac{54685}{9072}$$
$$-\frac{54685}{1134}\nu+\frac{54685}{567}\nu^2\Bigg]+\hat{\mu}_3^4\Bigg[\frac{6835}{254016}-\frac{6835}{31752}\nu+\frac{6835}{15876}\nu^2\Bigg]+\hat{\mu}_4^2\Bigg[-\frac{400}{3969}+\frac{800}{1323}\nu-\frac{400}{441}\nu^2\Bigg]$$
$$+\hat{\epsilon}_2{}^2\Bigg[-\frac{1570}{63}+\frac{7220}{63}\nu-\frac{3760}{63}\nu^2\Bigg]+\hat{\epsilon}_3{}^2\Bigg[-\frac{400}{63}+\frac{800}{21}\nu-\frac{400}{7}\nu^2\Bigg]+\hat{\epsilon}_2{}^4\Bigg[\frac{10}{81}-\frac{80}{81}\nu+\frac{160}{81}\nu^2\Bigg]\Bigg)\Bigg\}. \tag{2.16}$$

This parametrized multipolar phasing formula constitutes one of the most important results of the paper and forms the basis for the analysis which follows.

D. Multipole structure of the post-Newtonian phasing formula

We summarize in Table I the multipole structure of the PN phasing formula based on Eq. (2.16). The various multipoles which contribute to the different PN phasing terms are listed. The main features are as follows. As we go to higher PN orders, in addition to the higher order multipoles making an appearance, higher order PN corrections to the lower order multipoles also contribute. For example, mass quadrupole and its corrections (terms proportional to μ_2) appear at every PN order starting from 0PN. The 1.5PN and 3PN log terms contain only μ_2 and are due to the leading order tail effect [70] and tails of tails effect [71], respectively. The 3PN non-logarithmic term contains all the seven multipole coefficients.

Due to the aforementioned structure, it is evident that if one of the multipole moments is different from GR, it is likely to affect the phasing coefficients at more than one PN order. For instance, a deviation in μ_2 could result in dephasing of each one of the PN phasing coefficient. There are seven independent multipole coefficients which determine eight PN coefficients. The eight equations which relate the phasing terms to the multipoles are inadequate to extract all the seven multipoles. This is because three of the eight equations relate the PN coefficients only to μ_2, and another two relate the 1PN and 2.5PN logarithmic terms to a set of three multipole coefficients $\{\mu_2, \mu_3, \epsilon_2\}$. It turns out that, in principle, by independently measuring the eight PN coefficients, we can measure all the multipoles except μ_5 and ϵ_4. It is well-known that measuring all the eight phasing coefficients together provides very bad bounds [12, 13]. The version of the parametrized tests of Post-Newtonian theory, where we vary only one parameter at a time [13, 16], cannot be mapped to the multipole coefficients, as varying multipole moments will cause more than one PN order to change, which conflicts with the original assumption.

Though mapping the space of PN coefficients to that of the multipole coefficients is not possible, it is possible to relate the multipole deformations to that of the parametrized test. If, for instance, μ_2 is different from GR, it can lead to dephasing in one or more of the PN phasing terms depending on what

PN order	frequency dependences	Multipole coefficients
0 PN	$f^{-5/3}$	μ_2
1 PN	f^{-1}	μ_2, μ_3, ϵ_2
1.5 PN	$f^{-2/3}$	μ_2
2 PN	$f^{-1/3}$	$\mu_2, \mu_3, \mu_4, \epsilon_2, \epsilon_3$
2.5 PN log	$\log f$	μ_2, μ_3, ϵ_2
3 PN	$f^{1/3}$	$\mu_2, \mu_3, \mu_4, \mu_5, \epsilon_2, \epsilon_3, \epsilon_4$
3 PN log	$f^{1/3} \log f$	μ_2
3.5 PN	$f^{2/3}$	$\mu_2, \mu_3, \mu_4, \epsilon_2, \epsilon_3$

TABLE I. Summary of the multipolar structure of the PN phasing formula. Contribution of various multipoles to different phasing coefficients and their frequency dependences are tabulated. Following the definitions introduced in the paper, μ_l are associated to the deformations of mass-type multipole moments and ϵ_l refer to the deformations of current-type multipole moments.

the correction is to the mass quadrupole at different PN orders. This motivates, based on the multipolar structure, to perform parametrized tests of PN theory while varying simultaneously certain PN coefficients[1].

III. PARAMETER ESTIMATION OF THE MULTIPOLE COEFFICIENTS

In this section, we will set up the parameter estimation problem to measure the multipolar coefficients and present our forecasts for Advanced LIGO, Einstein Telescope, Cosmic Explorer and LISA. Using the frequency-domain gravitational waveform, we study how well the current and future generation of GW detectors can probe the multipolar structure of GR. To quantify this, we derive the projected accuracies with which various multipole moments may be measured for various detector configurations by using standard parameter estimation techniques. Following the philosophy of Refs. [12, 15, 16], while computing the errors we consider deviation of only one multipole at a time.

An ideal test would have been where all the coefficients are varied at the same time, but this will lead to almost no meaningful constraints because of the strong degeneracies among different coefficients. The proposed test, however, would not affect our ability to detect a potential deviation because in the multipole structure, a deviation of more than one multipole coefficients would invariably show up in the set of tests performed by varying one coefficient at a time [15–18].

We first use Fisher information matrix approach to derive the errors on the multipole coefficients. Fisher matrix is a useful semi-analytic method which uses a quadratic fit to the log-likelihood function to derive the $1-\sigma$ error bars on the parameters of the signal [54, 55, 92, 93]. Given a GW signal $\tilde{h}(f;\vec{\theta})$, which is described by the set of parameters $\vec{\theta}$, the Fisher information matrix is defined as

$$\Gamma_{mn} = \langle \tilde{h}_m, \tilde{h}_n \rangle, \tag{3.1}$$

where $\tilde{h}_m = \partial\tilde{h}(f;\vec{\theta})/\partial\theta_m$, and the angular bracket, $\langle ..., ... \rangle$, denotes the noise-weighted inner product defined by

$$\langle a, b \rangle = 2 \int_{f_{\rm low}}^{f_{\rm high}} \frac{a(f)\, b^*(f) + a^*(f)\, b(f)}{S_h(f)}\, df\,. \tag{3.2}$$

Here $S_h(f)$ is the one-sided noise power spectral density (PSD) of the detector and $[f_{\rm low}, f_{\rm high}]$ are the lower and upper limits of integration. The variance-covariance matrix is defined by the inverse of the Fisher matrix,

$$C^{mn} = (\Gamma^{-1})^{mn},$$

where the diagonal components, C^{mm}, are the variances of θ^m. The $1-\sigma$ errors on θ^m is, therefore, given as

$$\sigma^m = \sqrt{C^{mm}}\,. \tag{3.3}$$

Since Fisher matrix-based estimates are only reliable in the high signal-to-noise ratio limit [92, 94, 95], we spot check representative cases for consistency, with estimates based on a Bayesian inference algorithm that uses an MCMC method to sample the likelihood function. This method is not limited by the quadratic approximation to the log-likelihood and hence considered to be a more reliable estimate of measurement accuracies one might have in a real experiment. In this method we compute the probability distribution for the parameters implied by a signal $h(t)$ buried in the Gaussian noise $d(t) = h(t) + n(t)$ while incorporating our prior assumptions about the probability distribution for the parameters. The Bayes' rule states that the probability distribution for a set of model parameters $\vec{\theta}$ implied by data d is

$$p(\vec{\theta}|d) = \frac{p(d|\vec{\theta})\, p(\vec{\theta})}{p(d)}\,, \tag{3.4}$$

where $p(d|\vec{\theta})$ is called the *likelihood* function, which gives the probability of observing data d given the model parameter $\vec{\theta}$, defined as

$$p(d|\vec{\theta}) = \exp\left[-\frac{1}{2} \int_{f_{\rm low}}^{f_{\rm high}} \frac{|\tilde{d}(f) - \tilde{h}(f;\vec{\theta})|^2}{S_h(f)}\, df \right], \tag{3.5}$$

where $\tilde{d}(f)$ and $\tilde{h}(f;\vec{\theta})$ are the Fourier transform of $d(t)$ and $h(t)$, respectively. $p(\vec{\theta})$ is the *prior probability distribution* of parameters $\vec{\theta}$ and $p(d)$ is an overall normalization constant known as *evidence*,

$$p(d) = \int p(d|\vec{\theta})\, p(\vec{\theta})\, d\vec{\theta}\,. \tag{3.6}$$

In this paper, we use uniform prior on all the parameters we are interested in and used python-based MCMC sampler `emcee` [56] to sample the likelihood surface and get the posterior distribution for all the parameters.

[1] We thank Archisman Ghosh for pointing out this possibility to us.

We use noise PSDs of advanced LIGO (aLIGO) and Cosmic Explorer-wide band (CE-wb) [25], Einstein Telescope-D (ET-D) [96] as representatives of the current and next generation of ground-based GW interferometers and LISA. We use the noise PSD given in [96] for ET-D, analytical fits of PSDs given in [97] and [98] for aLIGO and LISA respectively, and the following fit for CE-wb noise PSD ,

$$S_h(f) = 5.62\times10^{-51} + 6.69\times10^{-50} f^{-0.125} + \frac{7.80\times10^{-31}}{f^{20}} + \frac{4.35\times10^{-43}}{f^{6}} + 1.63\times10^{-53} f + 2.44\times10^{-56} f^2 + 5.45\times10^{-66} f^5 \ \mathrm{Hz}^{-1}\,, \tag{3.7}$$

where f is in units of Hz. We compute the Fisher matrix (or likelihood in the Bayesian framework) considering the signal to be described by the set of parameters $\{\ln\mathcal{A}, \ln M_c, \ln\nu, t_c, \phi_c\}$ and the additional parameter μ_l or ϵ_l. In order to compute the inner product using Eq. (3.2), we assume $f_{\rm low}$ to be 20 Hz, 1 Hz, 5 Hz and 10^{-4} Hz for aLIGO, ET-D, CE-wb and LISA noise PSDs respectively. We choose $f_{\rm high}$ to be the frequency at the last stable circular orbit of a Schwarzschild BH with a total mass m given by $f_{\rm LSO} = 1/(\pi\, m\, 6^{3/2})$ for aLIGO, ET-D and CE-wb noise PSDs. For LISA, we choose the upper cut off frequency to be the minimum of $[0.1, f_{\rm LSO}]$.

All of the parameter estimations for aLIGO, CE-wb and LISA, we carry out here, assume detections of the signals with a single detector, where as for ET-D, due to it's triangular shape, we consider the noise PSD to be enhanced roughly by a factor of 1.5. As our aim is to estimate the intrinsic parameters of the signal, which directly affect the binary dynamics, the single detector estimates are good enough for our purposes and a network of detectors may improve it by the square root of the number of detectors. Hence the reported errors are likely to give rough, but conservative, estimates of the expected accuracies with which the multipole coefficients may be estimated.

IV. RESULTS AND DISCUSSION

In this section, we report the $1-\sigma$ measurement errors on the multipole coefficients introduced in the previous section, obtained using the Fisher matrix as well as Bayesian analysis and discuss their implications.

Our results for the four different detector configurations are presented in figures 1, 3 and 5 which show the errors on the various multipole coefficients μ_l, ϵ_l for aLIGO, ET-D, CE-wb and LISA, respectively. For all of these estimates we consider the sources at fixed distances. In addition to the intrinsic parameters there are four more (angular) parameters that are needed to completely specify the gravitational waveform. More specifically one needs two angles to define the location of the source on the sky and other two angles to specify the orientation of the orbital plane w.r.t the detector plane [8]. Since we are using a pattern averaged waveform [87] (i.e., a waveform averaged over all the four angles), the luminosity distance can be thought of as an *effective* distance which we assume to be 100 Mpc for aLIGO, ET-D and CE-wb, and 3 Gpc for LISA. For aLIGO, ET-D and CE-wb, we explore the bounds for the binaries with total mass in the range [1,70] $M_\odot$ and for LISA detections in the range $[10^4, 10^7]$ $M_\odot$.

A. Advanced LIGO

In Fig. 1 we show the projected 1-σ errors on the three leading order multipole moments, μ_2, μ_3 and ϵ_2, as a function of total mass of the binary for aLIGO noise PSD using the Fisher matrix. Different curves are for different mass ratios, $q = m_1/m_2 = 1.2$ (red), 2 (cyan) and 5 (blue). For the multipole coefficients considered, low mass systems obtain the smallest errors and hence the tightest constraints. This is expected as low mass systems live longer in the detector band and have larger number of cycles, thereby allowing us to measure the parameters very well. The bounds on μ_3 and ϵ_2, associated with the mass octupole and current quadrupole, increase monotonically with the total mass of the system for a given mass ratio. However, the bounds on μ_2 show a local minimum in the intermediate mass regime for smaller mass ratios. This is because, unlike other multipole parameters, μ_2 appears both in the amplitude and the phase of the signal. The derivative of the waveform with respect to μ_2 has contributions from both the amplitude and phase. Schematically, the Fisher matrix element is given by

$$\Gamma_{\mu_2\mu_2} \sim \int_{f_{\rm low}}^{f_{\rm upper}} \frac{\mathcal{A}^2 f^{-7/3}}{S_h(f)} \left(1 + \mu_2^2 \psi'^2\right) df, \tag{4.1}$$

where $\psi' = \partial\psi/\partial\mu_2$. As the inverse of this term dominantly determines the error on μ_2, the local minimum is a result of the trade-off between the contributions from the amplitude and the phase of the waveform. Interestingly, as we go to higher mass ratios, this feature disappears resulting in a monotonically increasing curve (such as for $q = 5$).

We find the mass multipole moments μ_2 and μ_3 are much better estimated as compared to the current multipole moment ϵ_2. Another important feature is that the bounds μ_3 and ϵ_2 are worse for equal mass binaries. Mass octupole and current quadrupole are odd parity multipole moments (unlike, say, mass quadrupole which is even)[2]. Every odd parity multipole moment comes with a mass asymmetry factor $\sqrt{1-4\nu}$ that vanishes in the equal mass limit, and hence the errors diverge. Consequently, the Fisher matrix becomes badly conditioned and the precision with which we recover these parameters appears to become very poor, but this is an artifact of the Fisher matrix.

In order to cross-check the validity of the Fisher matrix-based estimates, we performed a Bayesian analysis to find the posterior distribution of the three multipole parameters, for the same systems as in the Fisher matrix analysis. Moreover we considered flat prior probability distribution for all the six

[2] Mass-type multipoles with even l and current-type moments with odd l are considered 'even' and odd l mass multipoles and even l current moments are 'odd'.

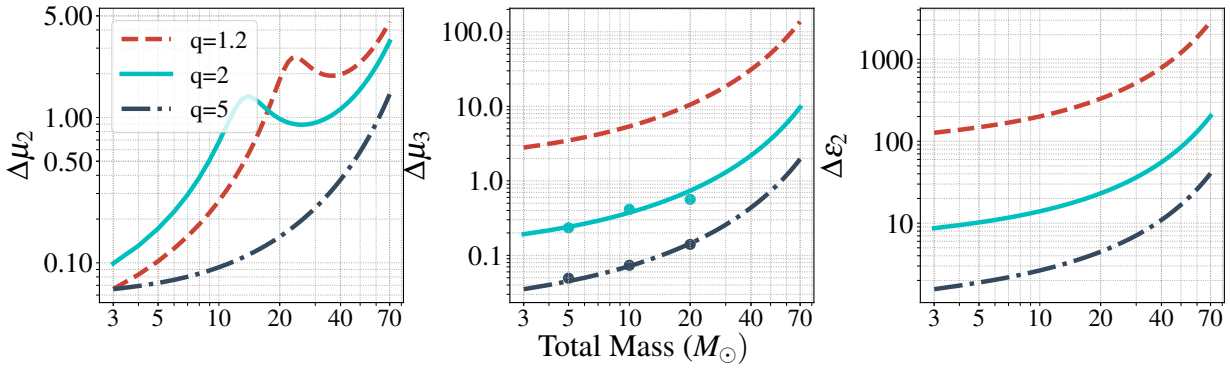

FIG. 1. Projected $1-\sigma$ errors on μ_2, μ_3 and ϵ_2 as a function of total mass for aLIGO noise PSD. Results from Bayesian analysis using MCMC sampling is given as dots showing good agreement. All the sources are considered to be at a fixed luminosity distance of 100 Mpc.

parameters $\{\ln\mathcal{A}, M_c, \nu, t_c, \phi_c, \mu_\ell$ or $\epsilon_\ell\}$ in a large enough range around their respective injection values. Given large number of iterations, once the MCMC chains are stabilized, we find good agreements with the Fisher estimates as in the case of μ_3 for $q = 2$ and 5, shown in Fig. 1. As an example, we present our results from MCMC analysis for μ_3 with $m = 5$ M$_\odot$ and $q = 2$, in the corner plots in Fig. 2. In Fig. 1 we see that the $1-\sigma$ errors in μ_3 from Fisher analysis agree very well with the MCMC results for $q = 2$ and 5. We did not find such an agreement for $q = 1.2$. We suspect that this is because for comparable mass systems the likelihood function, defined in Eq. (3.5), becomes shallow and it is computationally very difficult to find its maximum given a finite number of iterations. As a result, the MCMC chains did not converge and $1-\sigma$ bounds cannot be trusted for such cases. We find the non-convergence of MCMC chains for all the cases of μ_2 and ϵ_2 and hence we do not show those results in Fig. 1. To summarize, our findings indicate that one can only measure μ_2 and μ_3 with a good enough accuracy using aLIGO detectors.

B. Third generation detectors

Third generation detectors such as CE-wb (and ET-D) can place much better bounds on μ_2, μ_3 and ϵ_2 compared to aLIGO. Additionally, they can also measure μ_4 with reasonable accuracy, as shown by darker (and lighter) shaded curves in Fig. 3. The bounds on μ_2, μ_3 and ϵ_2 show similar trend as in the case of aLIGO except accuracy of the parameter estimation is much better overall. For few cases in low mass regime, μ_2 and μ_4 are better estimated for comparable mass binaries (i.e., $q = 1.2$). We also find that the bounds (represented by the lighter shaded curves in Fig. 3) obtained by using ET-D noise PSD are even better than the bounds from CE-wb, though the other features are more or less similar for both the detectors. This improvement in the precision of measurement is due to two reasons. The triangular shape of ET-D enhances the sensitivity roughly by a factor of 1.5 and its sensitivity is much better than CE-wb in the low frequency region.

For few representative cases, we compute errors in μ_2, ϵ_2 and μ_3 using Bayesian analysis and the results are shown as dots with the same color in Fig. 3. The MCMC results are in good agreement with the Fisher. Unlike aLIGO PSD, for CE-wb the MCMC chains converge quickly in the case of μ_2 and ϵ_2 because of the high signal-to-noise-ratios, which naturally lead to high likelihood values. As a result, it becomes relatively easier for the sampler to find the global maximum of the likelihood function in relatively fewer iterations. We also show an example corner plot for CE-wb PSD with $q = 2$, $m = 10$ M$_\odot$ in Fig. 4.

C. Laser Interferometer Space Antenna

In this Section, we discuss the projected errors on various multipole coefficients for the LISA detector. Here we consider four different mass ratios, $q = 1.2$ (red), 2 (cyan), 10 (blue) and 50 (green). The first three are representatives of comparable mass systems, while $q = 50$ refers to the intermediate mass ratio systems. We do not consider here the extreme mass ratio systems, the analysis of these systems needs phasing information at much higher PN orders such as in Ref. [99] which is beyond the scope of the present work. Moreover, in such systems, the motion of the smaller BH around the central compact object is expected to help us understand the multipolar structure of the central object and test its BH nature [33]. This is quite different from our objective here which is to use GW observations to understand the multipole structure of the gravitational field of the two-body problem in GR. The $q = 50$ case, in fact, falls in between these two classes and hence has a cleaner interpretation in our framework.

In Fig. 5 we show the projected bounds from the observations of supermassive BH mergers detectable by space-based LISA observatory. The error estimates for multipole moments with LISA are similar to that of CE-wb for mass ratios $q = 1.2$, 2. For $q = 10$ all the parameters except ϵ_4 are estimated very well. For $q = 50$, we find that LISA will be able to measure all the seven multipole coefficients with good accuracy. It is not entirely clear whether PN model is accurate enough for detection and parameter estimation of super massive binary

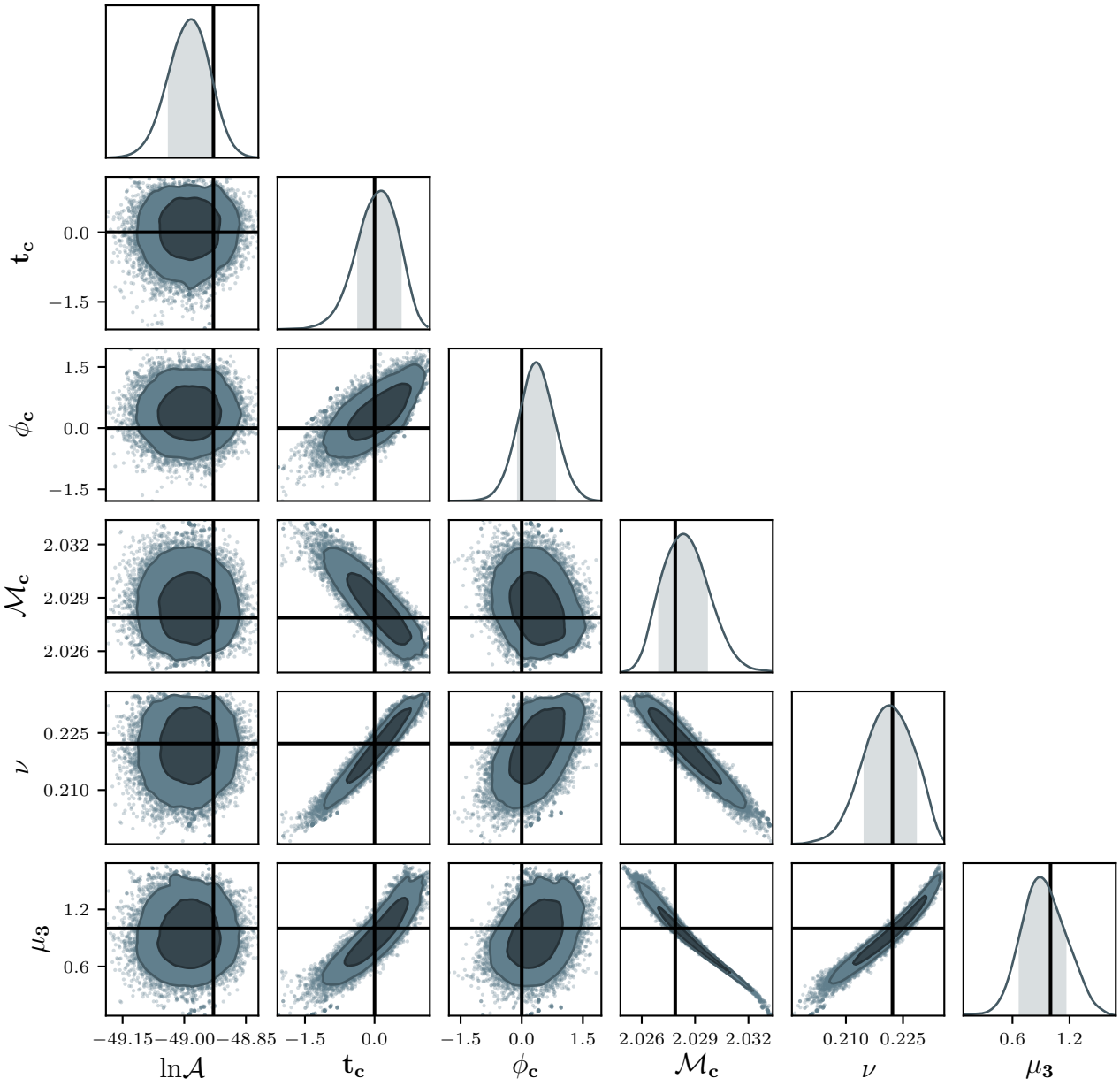

FIG. 2. The posterior distributions of all the six parameters $\{\ln\mathcal{A}, t_c, \phi_c, \mathcal{M}_c, \nu, \mu_3\}$ and their corresponding contour plots obtained from the MCMC experiments (see Sec. III for details) for a compact binary system at a distance of 100 Mpc with q=2, m = 5 $M_\odot$ using the noise PSD of aLIGO. The darker shaded region in the posterior distributions as well as in the contour plots shows the 1-σ bounds on the respective parameters.

BHs with $q = 50$, for which the number of GW cycles could be an order of magnitude higher than it is for equal mass configurations. However our findings carry importance as it points to the huge potential such systems have for fundamental physics.

To summarize, we find, in general, that even parity multipoles (i.e., μ_2 and μ_4) are better measured when the binary constituents are of equal or comparable masses, whereas the odd multipoles (i.e., μ_3, μ_5, ϵ_2 and ϵ_3) are better measured when the binary has mass asymmetry. This is because the even multipoles are proportional to the symmetric mass ratio ν, whereas the odd ones are proportional to the mass asymmetry $\sqrt{1-4\nu}$, which identically vanishes for equal mass systems (see, e.g., Eq. (4.4) of [52]).

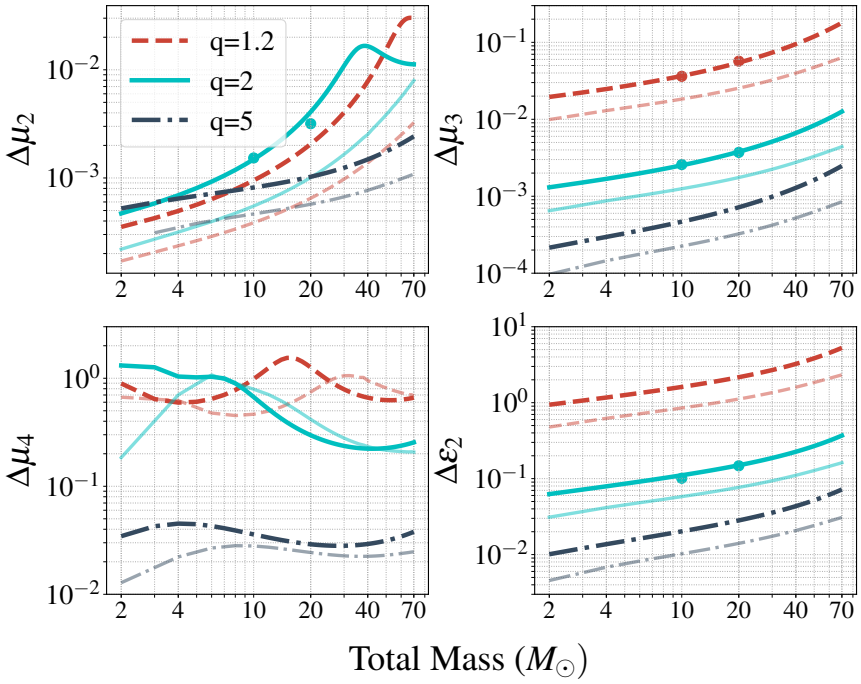

FIG. 3. Dark shaded curves correspond to the projected $1-\sigma$ error bars on μ_2, μ_3, μ_4 and ϵ_2 using the proposed CE-wb noise PSD as a function of total mass, where as lighter shades denote the bounds obtained using ET-D noise PSD. All the sources are considered to be at a fixed luminosity distance of 100 Mpc. The higher order multipole moments such as μ_4 and ϵ_2 cannot be measured well using aLIGO hence it may be a unique science goal of the third generation detectors.

V. SUMMARY AND FUTURE DIRECTIONS

We have proposed a novel way to test for possible deviation from GR using GW observations from compact binaries by probing the multipolar structure of the GW phasing in any alternative theories of gravity. We compute a parametrized multipolar GW phasing formula that can be used to probe potential deviations from the multipolar structure of GR. Using Fisher information matrix and Bayesian parameter estimation, we predict the accuracies with which the multipole coefficients could be measured from GW observations with present and future detectors. We find that the space mission LISA, currently under development, can measure all the multipoles of the compact binary system making it a unique fundamental science that LISA will be able to deliver.

In deriving the parametrized multipolar phasing formula, we have assumed that the conservative dynamics of the binary follow the predictions of GR. In the appendix, we have provided a phasing formula where we also deform the PN terms in the orbital energy of the binary. This should be seen as a first step towards a more complete parametrized phasing where we separate the conservative and dissipative contributions to the phasing. A systematic revisit of the problem starting from the foundations of PN theory as applied to the compact binary is needed to obtain a complete phasing formula parametrizing uniquely the conservative and dissipative sectors in the phasing formula. This we postpone for a follow up work.

The present results using non-spinning waveforms should be considered to be a proof-of-principle demonstration, to be followed up with a more realistic waveform that accounts for spin effects, effects of orbital eccentricity and higher modes. Incorporation of the proposed test in the framework of Effective One-Body formalism [100] is also among the future directions we plan to pursue. There are ongoing efforts to implement this method in the framework of LALInference [101] so that it can be applied on the compact binaries detected by advanced LIGO and Virgo detectors.

ACKNOWLEDGEMENT

SK and KGA thank B. Iyer, G. Faye, A. Ashtekar, G. Date, A. Ghosh and J. Hoque for several useful discussions and N. V. Krishnendu for cross-checking some of the calculations reported here. We thank B. Iyer for useful comments and suggestions on the manuscript as part of the internal review of the LIGO and Virgo Collaboration, which has helped us improve the presentation. KGA, AG, SK and BSS acknowledge the support by the Indo-US Science and Technology Forum through the Indo-US Centre for the Exploration of Extreme

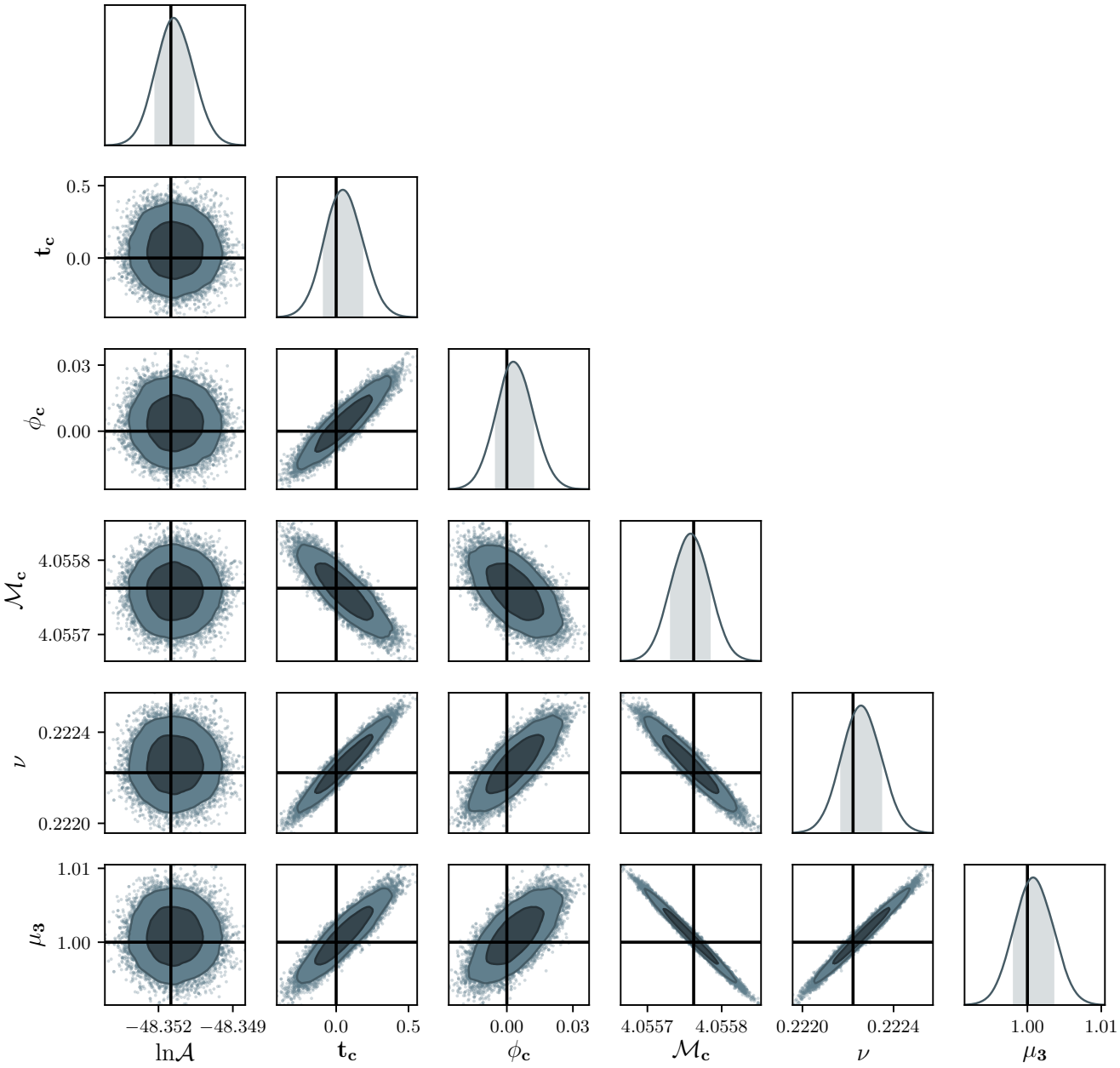

FIG. 4. The posterior distributions of all the six parameters $\{\ln\mathcal{A}, t_c, \phi_c, \mathcal{M}_c, \nu, \mu_3\}$ and their corresponding contour plots obtained from the MCMC experiments (see Sec. III for details) for a compact binary system at a distance of 100 Mpc with q=2, m = 10 $M_\odot$ using the noise PSD of CE-wb. The darker shaded region in the posterior distributions as well as in the contour plots shows the 1-σ bounds on the respective parameters.

Gravity, grant IUSSTF/JC-029/2016. AG and BSS are supported in part by NSF grants PHY-1836779, AST-1716394 and AST-1708146. KGA is partially support by a grant from Infosys Foundation. KGA also acknowledge partial support by the grant EMR/2016/005594. CVdB is supported by the research programme of the Netherlands Organisation for Scientific Research (NWO). Computing resources for this project were provided by the Pennsylvania State University. This document has LIGO preprint number P1800274.

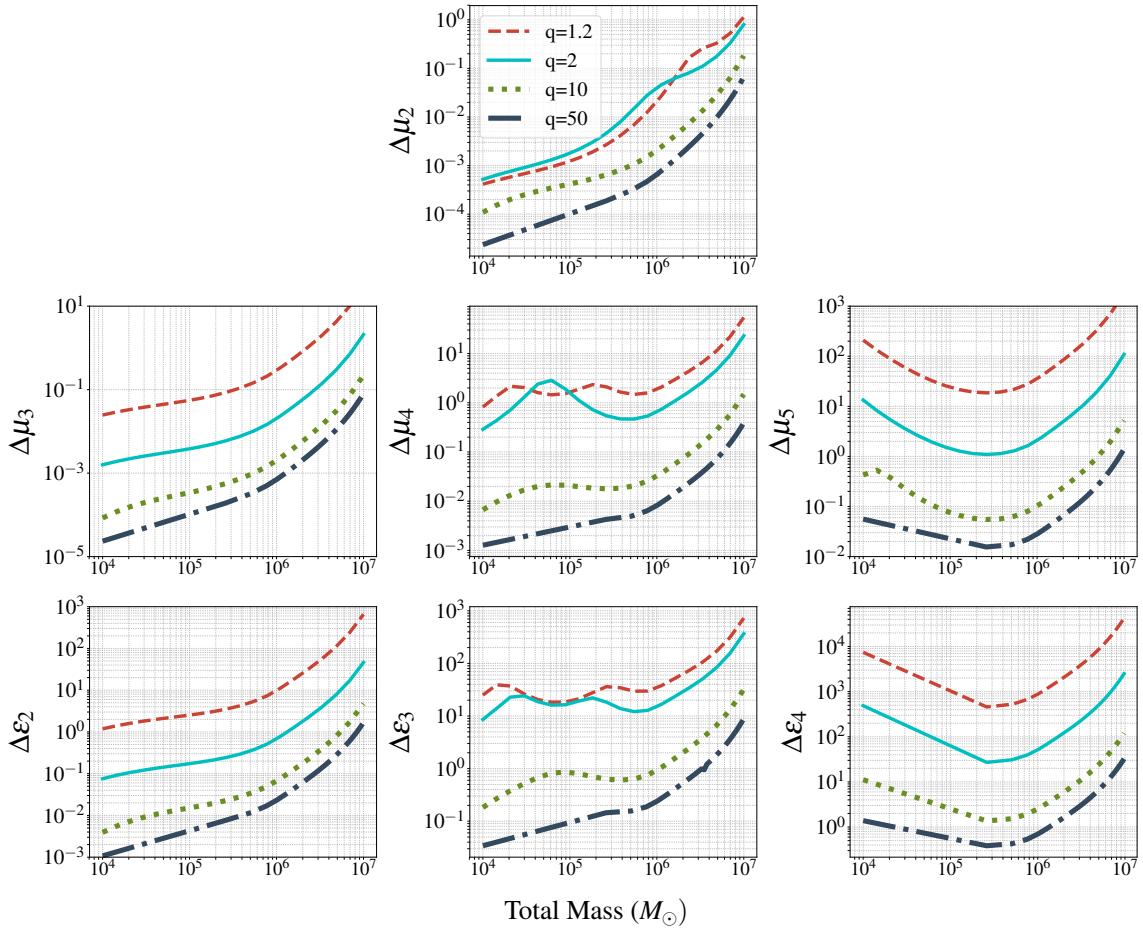

FIG. 5. Projected constraints on various multipole coefficients using LISA sensitivity, as a function of total mass of the binary. All the sources are considered to be at a fixed luminosity distance of 100 Mpc. LISA can measure all the seven multipoles which contribute to the phasing and hence will be able to place extremely stringent bounds on the multipoles of the compact binary gravitational field.

Appendix: Frequency domain phasing formula allowing for the deformation of conservative dynamics

Binding energy parametrized at each PN order by four different constants $\{\alpha_0, \alpha_1, \alpha_2, \alpha_3\}$ used in the computation of parametrized GW phasing considering deviation in the conserved energy (mentioned in Sec. II B), is given by

$$E(v) = -\frac{1}{2}\nu v^2\left[\alpha_0 - \left(\frac{3}{4}+\frac{1}{12}\nu\right)\alpha_1 v^2 - \left(\frac{27}{8}-\frac{19}{8}\nu+\frac{1}{24}\nu^2\right)\alpha_2 v^4 - \left\{\frac{675}{64} - \left(\frac{34445}{576}-\frac{205}{96}\pi^2\right)\nu + \frac{155}{96}\nu^2 + \frac{35}{5184}\nu^3\right\}\alpha_3 v^6\right]. \tag{A.1}$$

The resulting phase is quoted below,

$$\psi(f) = 2\pi f t_c - \frac{\pi}{4} - \phi_c + \frac{3\alpha_0}{128 v^5 \mu_2^2 \nu}\left\{1 + v^2\left(\frac{2140}{189} - \frac{1100}{189}\nu - \frac{\alpha_1}{\alpha_0}\left[\frac{10}{3}+\frac{10}{27}\nu\right] + \hat{\mu}_3^2\left[-\frac{6835}{2268}+\frac{6835}{567}\nu\right] + \hat{\epsilon}_2{}^2\left[-\frac{5}{81}+\frac{20}{81}\nu\right]\right)\right.$$
$$\left. -16\pi v^3 + v^4\left(\frac{295630}{1323} - \frac{267745}{2646}\nu + \frac{32240}{1323}\nu^2 + \frac{\alpha_1}{\alpha_0}\left[-\frac{535}{7}+\frac{1940}{63}\nu+\frac{275}{63}\nu^2\right] + \frac{\alpha_2}{\alpha_0}\left[-\frac{405}{4}+\frac{285}{4}\nu-\frac{5}{4}\nu^2\right]\right.\right.$$

$$
\begin{aligned}
&+\hat{\mu}_3^2\left[-\frac{104815}{3528}+\frac{8545}{63}\nu-\frac{29630}{441}\nu^2+\frac{\alpha_1}{\alpha_0}\left(\frac{6835}{336}-\frac{34175}{432}\nu-\frac{6835}{756}\nu^2\right)\right]+\hat{\mu}_3^2{\hat{\epsilon}_2}^2\left[\frac{6835}{9072}-\frac{6835}{1134}\nu+\frac{6835\nu^2}{567}\right]\\
&+\hat{\mu}_3^4\left[\frac{9343445}{508032}-\frac{9343445}{63504}\nu+\frac{9343445}{31752}\nu^2\right]+\hat{\mu}_4^2\left[-\frac{89650}{3969}+\frac{179300}{1323}\nu-\frac{89650}{441}\nu^2\right]+{\hat{\epsilon}_2}^2\left[-\frac{1885}{756}+\frac{695}{63}\nu\right.\\
&\left.-\frac{800}{189}\nu^2+\frac{\alpha_1}{\alpha_0}\left(\frac{5}{12}-\frac{175}{108}\nu-\frac{5}{27}\nu^2\right)\right]+{\hat{\epsilon}_2}^4\left[\frac{5}{648}-\frac{5}{81}\nu+\frac{10}{81}\nu^2\right]+{\hat{\epsilon}_3}^2\left[-\frac{50}{63}+\frac{100}{21}\nu-\frac{50}{7}\nu^2\right]\Bigg)\\
&+\pi v^5\left(3\log\left[\frac{v}{v_{\rm LSO}}\right]+1\right)\left(\frac{80}{189}\left[214-131\nu\right]-\frac{80\alpha_1}{27\alpha_0}\left[9+\nu\right]-\frac{9115}{756}\hat{\mu}_3^2\left[1-4\nu\right]-\frac{20}{27}{\hat{\epsilon}_2}^2\left[1-4\nu\right]\right)\\
&+v^6\left(\frac{36847016}{509355}-\frac{640}{3}\pi^2-\frac{6848}{21}\gamma_E-\frac{6848}{21}\log[4v]+\left[\frac{28398155}{67914}+\frac{205}{12}\pi^2\right]\nu-\frac{563225}{3773}\nu^2+\frac{3928700}{305613}\nu^3\right.\\
&+\frac{\alpha_1}{\alpha_0}\left[\frac{295630}{441}-\frac{1818445}{7938}\nu+\frac{312575}{7938}\nu^2+\frac{32240}{3969}\nu^3\right]+\frac{\alpha_2}{\alpha_0}\left[\frac{14445}{14}-\frac{8795}{7}\nu+\frac{8105}{21}\nu^2-\frac{275}{42}\nu^3\right]\\
&+\frac{\alpha_3}{\alpha_0}\left[\frac{3375}{4}+\left(-\frac{172225}{36}+\frac{1025}{6}\pi^2\right)\nu+\frac{775}{6}\nu^2+\frac{175}{324}\nu^3\right]+\hat{\mu}_3^2\left[\frac{732782515}{3667356}-\frac{1061322545}{1222452}\nu+\frac{1027073335}{3667356}\nu^2\right.\\
&-\frac{15723035}{916839}\nu^3+\frac{\alpha_1}{\alpha_0}\left(-\frac{104815}{1176}+\frac{4201865}{10584}\nu-\frac{206855}{1323}\nu^2-\frac{29630}{1323}\nu^3\right)+\frac{\alpha_2}{\alpha_0}\left(-\frac{61515}{224}+\frac{868045}{672}\nu-\frac{1565215}{2016}\nu^2\right.\\
&\left.\left.+\frac{6835}{504}\nu^3\right)\right]+\hat{\mu}_3^2{\hat{\epsilon}_2}^2\left[-\frac{1742995}{190512}+\frac{1045805}{13608}\nu-\frac{2091650}{11907}\nu^2+\frac{697310}{11907}\nu^3+\frac{\alpha_1}{\alpha_0}\left(\frac{6835}{3024}-\frac{485285}{27216}\nu+\frac{116195}{3402}\nu^2+\frac{6835}{1701}\nu^3\right)\right]\\
&+\hat{\mu}_3^2{\hat{\epsilon}_2}^4\left[\frac{6835}{108864}-\frac{6835}{9072}\nu+\frac{6835}{2268}\nu^2-\frac{6835}{1701}\nu^3\right]+\hat{\mu}_3^2{\hat{\epsilon}_3}^2\left[-\frac{34175}{7938}+\frac{170875}{3969}\nu-\frac{375925}{2646}\nu^2+\frac{68350}{441}\nu^3\right]\\
&+\hat{\mu}_3^2\hat{\mu}_4^2\left[-\frac{61275775}{500094}+\frac{306378875}{250047}\nu-\frac{674033525}{166698}\nu^2+\frac{122551550}{27783}\nu^3\right]+\hat{\mu}_3^4\left[\frac{140055985}{5334336}-\frac{1148286835}{5334336}\nu+\frac{307950925}{666792}\nu^2\right.\\
&\left.-\frac{27838955}{333396}\nu^3+\frac{\alpha_1}{\alpha_0}\left(\frac{9343445}{169344}-\frac{663384595}{1524096}\nu+\frac{158838565}{190512}\nu^2+\frac{9343445}{95256}\nu^3\right)\right]+\hat{\mu}_3^4{\hat{\epsilon}_2}^2\left[\frac{9343445}{3048192}-\frac{9343445}{254016}\nu\right.\\
&\left.+\frac{9343445}{63504}\nu^2-\frac{9343445}{47628}\nu^3\right]+\hat{\mu}_3^6\left[\frac{12772489315}{256048128}-\frac{12772489315}{21337344}\nu+\frac{12772489315}{5334336}\nu^2-\frac{12772489315}{4000752}\nu^3\right]\\
&+\hat{\mu}_4^2\left[-\frac{24426860}{916839}+\frac{62508560}{305613}\nu-\frac{12980600}{33957}\nu^2+\frac{286700}{11319}\nu^3+\frac{\alpha_1}{\alpha_0}\left(-\frac{89650}{1323}+\frac{4751450}{11907}\nu-\frac{2241250}{3969}\nu^2-\frac{89650}{1323}\nu^3\right)\right]\\
&+\hat{\mu}_4^2{\hat{\epsilon}_2}^2\left[-\frac{89650}{35721}+\frac{896500}{35721}\nu-\frac{986150}{11907}\nu^2+\frac{358600\nu^3}{3969}\right]+\hat{\mu}_5^2\left[\frac{1002569}{12474}-\frac{4010276}{6237}\nu+\frac{10025690}{6237}\nu^2-\frac{8020552}{6237}\nu^3\right]\\
&+{\hat{\epsilon}_2}^2\left[\frac{6134935}{190512}-\frac{2353285}{15876}\nu+\frac{550075}{6804}\nu^2-\frac{150845}{11907}\nu^3+\frac{\alpha_1}{\alpha_0}\left(-\frac{1885}{252}+\frac{73175}{2268}\nu-\frac{1705}{189}\nu^2-\frac{800}{567}\nu^3\right)\right.\\
&\left.+\frac{\alpha_2}{\alpha_0}\left(-\frac{45}{8}+\frac{635}{24}\nu-\frac{1145}{72}\nu^2+\frac{5}{18}\nu^3\right)\right]+{\hat{\epsilon}_2}^2{\hat{\epsilon}_3}^2\left[-\frac{50}{567}+\frac{500}{567}\nu-\frac{550}{189}\nu^2+\frac{200}{63}\nu^3\right]+{\hat{\epsilon}_2}^4\left[-\frac{25}{126}+\frac{3775}{2268}\nu-\frac{2150}{567}\nu^2\right.\\
&\left.+\frac{100}{81}\nu^3+\frac{\alpha_1}{\alpha_0}\left(\frac{5}{216}-\frac{355}{1944}\nu+\frac{85}{243}\nu^2+\frac{10}{243}\nu^3\right)\right]+{\hat{\epsilon}_2}^6\left[\frac{5}{11664}-\frac{5}{972}\nu+\frac{5}{243}\nu^2-\frac{20}{729}\nu^3\right]+{\hat{\epsilon}_3}^2\left[\frac{37180}{3969}-\frac{235640}{3969}\nu\right.\\
&\left.+\frac{420200}{3969}\nu^2-\frac{47900}{1323}\nu^3+\frac{\alpha_1}{\alpha_0}\left(-\frac{50}{21}+\frac{2650}{189}\nu-\frac{1250}{63}\nu^2-\frac{50}{21}\nu^3\right)\right]+{\hat{\epsilon}_4}^2\left[\frac{5741}{1764}-\frac{11482}{441}\nu+\frac{28705}{441}\nu^2-\frac{22964}{441}\nu^3\right]\Bigg)\\
&+\pi v^7\left(\frac{2365040}{1323}-\frac{1300930}{1323}\nu+\frac{400930}{1323}\nu^2+\frac{\alpha_1}{\alpha_0}\left[-\frac{4280}{7}+\frac{19300}{63}\nu+\frac{2620}{63}\nu^2\right]+\frac{\alpha_2}{\alpha_0}\left(-810+570\nu-10\nu^2\right)\right.\\
&+\hat{\mu}_3^2\left[-\frac{69905}{588}+\frac{191495}{336}\nu-\frac{73995}{196}\nu^2+\frac{\alpha_1}{\alpha_0}\left(\frac{9115}{112}-\frac{45575}{144}\nu-\frac{9115}{252}\nu^2\right)\right]+\hat{\mu}_3^2{\hat{\epsilon}_2}^2\left[\frac{54685}{9072}-\frac{54685}{1134}\nu+\frac{54685}{567}\nu^2\right]\\
&+\hat{\mu}_3^4\left[\frac{6835}{254016}-\frac{6835}{31752}\nu+\frac{6835}{15876}\nu^2\right]+\hat{\mu}_4^2\left[-\frac{400}{3969}+\frac{800}{1323}\nu-\frac{400}{441}\nu^2\right]+{\hat{\epsilon}_2}^2\left[-\frac{1885}{63}+\frac{2815}{21}\nu-\frac{3620}{63}\nu^2\right.\\
&\left.\left.\left.+\frac{\alpha_1}{\alpha_0}\left(5-\frac{175}{9}\nu-\frac{20}{9}\nu^2\right)\right]+{\hat{\epsilon}_3}^2\left[-\frac{400}{63}+\frac{800}{21}\nu-\frac{400}{7}\nu^2\right]+{\hat{\epsilon}_2}^4\left[\frac{10}{81}-\frac{80}{81}\nu+\frac{160}{81}\nu^2\right]\right)\right\}. \qquad \text{(A.2)}
\end{aligned}
$$

The GW phasing for compact binaries can be represented by various PN approximants depending on the differences in which they treat the energy and flux functions. We redirect the reader to Refs. [88, 102] for a detailed discussion of these various approximants. We provide the input functions required for the computation of the phasing for TaylorT2, TaylorT3 and TaylorT4 in a Mathematica file (supl-Multipole.m) which serves the supplemental material to this paper. We closely follow the notations of [88] in this file.

[1] B. P. Abbott et al. (Virgo, LIGO Scientific), Phys. Rev. Lett. **116**, 061102 (2016), 1602.03837.
[2] B. P. Abbott et al. (Virgo, LIGO Scientific), Phys. Rev. Lett. **116**, 241103 (2016), 1606.04855.
[3] B. P. Abbott et al., Phys. Rev. Lett. **118**, 221101 (2017), 1706.01812.
[4] B. P. Abbott et al. (Virgo, LIGO Scientific), Phys. Rev. Lett. **119**, 141101 (2017), 1709.09660.
[5] B. Abbott et al., Phys. Rev. Lett. **119**, 161101 (2017), 1710.05832.
[6] T. L. S. Collaboration, J. Aasi, B. P. Abbott, R. Abbott, T. Abbott, M. R. Abernathy, K. Ackley, C. Adams, T. Adams, P. Addesso, et al., Classical and Quantum Gravity **32**, 074001 (2015).
[7] F. Acernese, M. Agathos, K. Agatsuma, D. Aisa, N. Allemandou, A. Allocca, J. Amarni, P. Astone, G. Balestri, G. Ballardin, et al., Classical and Quantum Gravity **32**, 024001 (2015).
[8] B. Sathyaprakash and B. Schutz, Living Rev.Rel. **12**, 2 (2009), arXiv:0903.0338.
[9] N. Yunes and X. Siemens, Living Rev. Rel. **16**, 9 (2013), 1304.3473.
[10] B. P. Abbott et al. (Virgo, LIGO Scientific), Phys. Rev. Lett. **116**, 221101 (2016), 1602.03841.
[11] B. P. Abbott et al. (Virgo, LIGO Scientific), Phys. Rev. **X6**, 041015 (2016), 1606.04856.
[12] K. G. Arun, B. R. Iyer, M. S. S. Qusailah, and B. S. Sathyaprakash, Class. Quantum Grav. **23**, L37 (2006), gr-qc/0604018.
[13] K. G. Arun, B. R. Iyer, M. S. S. Qusailah, and B. S. Sathyaprakash, Phys. Rev. D **74**, 024006 (2006), gr-qc/0604067.
[14] N. Yunes and F. Pretorius, Phys. Rev. D **80**, 122003 (2009), 0909.3328.
[15] C. K. Mishra, K. G. Arun, B. R. Iyer, and B. S. Sathyaprakash, Phys. Rev. **D 82**, 064010 (2010), 1005.0304.
[16] M. Agathos, W. Del Pozzo, T. G. F. Li, C. V. D. Broeck, J. Veitch, et al., Phys.Rev. **D89**, 082001 (2014), 1311.0420.
[17] T. G. F. Li, W. Del Pozzo, S. Vitale, C. Van Den Broeck, M. Agathos, J. Veitch, K. Grover, T. Sidery, R. Sturani, and A. Vecchio, Phys. Rev. **D85**, 082003 (2012), 1110.0530.
[18] J. Meidam et al., Phys. Rev. **D97**, 044033 (2018), 1712.08772.
[19] C. M. Will, Phys. Rev. D **57**, 2061 (1998), gr-qc/9709011.
[20] S. Mirshekari, N. Yunes, and C. M. Will, Phys. Rev. D **85**, 024041 (2012), 1110.2720.
[21] A. Ghosh et al., Phys. Rev. **D94**, 021101 (2016), 1602.02453.
[22] B. P. Abbott et al. (Virgo, Fermi-GBM, INTEGRAL, LIGO Scientific), Astrophys. J. **848**, L13 (2017), 1710.05834.
[23] N. Yunes, K. Yagi, and F. Pretorius, Phys. Rev. **D94**, 084002 (2016), 1603.08955.
[24] M. Abernathy et al., Einstein gravitational wave Telescope: Conceptual Design Study (Document number ET-0106A-10) (2010), ET-0106A-10.
[25] B. P. Abbott et al. (LIGO Scientific), Class. Quant. Grav. **34**, 044001 (2017), 1607.08697.
[26] http://lisa.jpl.nasa.gov.
[27] M. C. Miller and E. J. M. Colbert, Int. J. Mod. Phys. **D13**, 1 (2004), astro-ph/0308402.
[28] R. P. van der Marel, in Carnegie Observatories Centennial Symposium. 1. Coevolution of Black Holes and Galaxies Pasadena, California, October 20- (2003), astro-ph/0302101.
[29] J. M. Fregeau, S. L. Larson, M. C. Miller, R. W. O'Shaughnessy, and F. A. Rasio, Astrophys. J. **646**, L135 (2006), astro-ph/0605732.
[30] P. B. Graff, A. Buonanno, and B. S. Sathyaprakash, Phys. Rev. **D92**, 022002 (2015), 1504.04766.
[31] D. A. Brown, H. Fang, J. R. Gair, C. Li, G. Lovelace, I. Mandel, and K. S. Thorne, Phys. Rev. Lett. **99**, 201102 (2007), gr-qc/0612060.
[32] K. Chamberlain and N. Yunes, Phys. Rev. **D96**, 084039 (2017), 1704.08268.
[33] F. Ryan, Phys. Rev. D **56**, 1845 (1997).
[34] K. S. Thorne, in Particle and nuclear astrophysics and cosmology in the next millennium. Proceedings, Summer Study, Snowmass, USA, June 29-July (1995), pp. 0160–184, gr-qc/9506086.
[35] B. F. Schutz, Classical and Quantum Gravity **13**, A219 (1996).
[36] J. R. Gair, M. Vallisneri, S. L. Larson, and J. G. Baker, Living Rev. Rel. **16**, 7 (2013), 1212.5575.
[37] E. Berti, E. Barausse, V. Cardoso, L. Gualtieri, P. Pani, U. Sperhake, L. C. Stein, N. Wex, K. Yagi, T. Baker, et al., Classical and Quantum Gravity **32**, 243001 (2015), 1501.07274.
[38] K. G. Arun and A. Pai, Int.J.Mod.Phys. D **22**, 1341012 (2013), 1302.2198.
[39] G. F. Giudice, M. McCullough, and A. Urbano, JCAP **1610**, 001 (2016), 1605.01209.
[40] C. Chirenti and L. Rezzolla, Phys. Rev. **D94**, 084016 (2016), 1602.08759.
[41] V. Cardoso, E. Franzin, and P. Pani, Phys. Rev. Lett. **116**, 171101 (2016), 1602.07309.
[42] V. Cardoso, E. Franzin, A. Maselli, P. Pani, and G. Raposo, Phys. Rev. **D95**, 084014 (2017), [Addendum: Phys. Rev.D95,no.8,089901(2017)], 1701.01116.
[43] N. K. Johnson-Mcdaniel, A. Mukherjee, R. Kashyap, P. Ajith, W. Del Pozzo, and S. Vitale (2018), 1804.08026.
[44] N. V. Krishnendu, K. G. Arun, and C. K. Mishra, Phys. Rev. Lett. **119**, 091101 (2017), 1701.06318.
[45] S. Dhanpal, A. Ghosh, A. K. Mehta, P. Ajith, and B. S. Sathyaprakash (2018), 1804.03297.
[46] N. V. Krishnendu, C. K. Mishra, and K. G. Arun (2018), 1811.00317.

[47] L. Blanchet, Living Rev. Rel. **17**, 2 (2014), 1310.1528.
[48] F. Pretorius (2007), relativistic Objects in Compact Binaries: From Birth to Coalescence Editor: Colpi et al., arXiv:0710.1338.
[49] M. Sasaki and H. Tagoshi, Living Rev. Rel. **6**, 6 (2003), gr-qc/0306120.
[50] L. Blanchet and B. S. Sathyaprakash, Class. Quantum Grav. **11**, 2807 (1994).
[51] L. Blanchet and B. S. Sathyaprakash, Phys. Rev. Lett. **74**, 1067 (1995).
[52] L. Blanchet, T. Damour, and B. R. Iyer, Phys. Rev. D **51**, 5360 (1995), gr-qc/9501029.
[53] S. Endlich, V. Gorbenko, J. Huang, and L. Senatore, JHEP **09**, 122 (2017), 1704.01590.
[54] C. Rao, Bullet. Calcutta Math. Soc **37**, 81 (1945).
[55] H. Cramer, Mathematical methods in statistics (Pergamon Press, Princeton University Press, NJ, U.S.A., 1946).
[56] D. Foreman-Mackey, D. W. Hogg, D. Lang, and J. Goodman, Publications of the Astronomical Society of the Pacific **125**, 306 (2013), 1202.3665.
[57] K. Thorne, Rev. Mod. Phys. **52**, 299 (1980).
[58] L. Blanchet and T. Damour, Phys. Lett. A **104**, 82 (1984).
[59] L. Blanchet and T. Damour, Phil. Trans. Roy. Soc. Lond. A **320**, 379 (1986).
[60] L. Blanchet, Proc. Roy. Soc. Lond. A **409**, 383 (1987).
[61] L. Blanchet and T. Damour, Phys. Rev. D **37**, 1410 (1988).
[62] L. Blanchet and T. Damour, Annales Inst. H. Poincaré Phys. Théor. **50**, 377 (1989).
[63] L. Blanchet and T. Damour, Phys. Rev. D **46**, 4304 (1992).
[64] L. Blanchet, Phys. Rev. D **51**, 2559 (1995), gr-qc/9501030.
[65] L. Blanchet, B. R. Iyer, and B. Joguet, Phys. Rev. D **65**, 064005 (2002), Erratum-ibid **71**, 129903(E) (2005), gr-qc/0105098.
[66] T. Damour, P. Jaranowski, and G. Schäfer, Phys. Lett. B **513**, 147 (2001).
[67] L. Blanchet, T. Damour, G. Esposito-Farèse, and B. R. Iyer, Phys. Rev. Lett. **93**, 091101 (2004), gr-qc/0406012.
[68] T. Damour and B. R. Iyer, Phys. Rev. D **43**, 3259 (1991).
[69] L. Blanchet and T. Damour, Phys. Rev. **D37**, 1410 (1988).
[70] L. Blanchet and G. Schaefer, Class. Quant. Grav. **10**, 2699 (1993).
[71] L. Blanchet, Class. Quantum Grav. **15**, 113 (1998), gr-qc/9710038.
[72] L. Blanchet, Class. Quantum Grav. **15**, 89 (1998), gr-qc/9710037.
[73] D. Christodoulou, Phys. Rev. Lett. **67**, 1486 (1991).
[74] K. Thorne, Phys. Rev. D **45**, 520 (1992).
[75] K. G. Arun, L. Blanchet, B. R. Iyer, and M. S. S. Qusailah, Class. Quantum Grav. **21**, 3771 (2004), erratum-ibid. **22**, 3115 (2005), gr-qc/0404185.
[76] M. Favata, Phys. Rev. D **80**, 024002 (2009), 0812.0069.
[77] L. Blanchet, T. Damour, B. R. Iyer, C. M. Will, and A. G. Wiseman, Phys. Rev. Lett. **74**, 3515 (1995), gr-qc/9501027.
[78] L. Blanchet, G. Faye, B. R. Iyer, and B. Joguet, Phys. Rev. D **65**, 061501(R) (2002), Erratum-ibid **71**, 129902(E) (2005), gr-qc/0105099.
[79] L. Blanchet and B. R. Iyer, Class. Quantum Grav. **20**, 755 (2003), gr-qc/0209089.
[80] L. Blanchet, T. Damour, and G. Esposito-Farèse, Phys. Rev. D **69**, 124007 (2004), gr-qc/0311052.
[81] T. Damour, P. Jaranowski, and G. Schäfer, Phys. Rev. D **63**, 044021 (2001), erratum-ibid **66**, 029901(E) (2002).
[82] V. de Andrade, L. Blanchet, and G. Faye, Class. Quantum Grav. **18**, 753 (2001).
[83] Y. Itoh and T. Futamase, Phys. Rev. D **68**, 121501(R) (2003).
[84] L. Blanchet, Phys. Rev. D **54**, 1417 (1996), Erratum-ibid.**71**, 129904(E) (2005), gr-qc/9603048.
[85] B. R. Iyer and C. M. Will, Phys. Rev. Lett. **70**, 113 (1993).
[86] B. R. Iyer and C. M. Will, Phys. Rev. D **52**, 6882 (1995).
[87] T. Damour, B. R. Iyer, and B. S. Sathyaprakash, Phys. Rev. D **62**, 084036 (2000), gr-qc/0001023.
[88] A. Buonanno, B. Iyer, E. Ochsner, Y. Pan, and B. S. Sathyaprakash, Phys. Rev. **D80**, 084043 (2009), 0907.0700.
[89] B. S. Sathyaprakash and S. V. Dhurandhar, Phys. Rev. **D44**, 3819 (1991).
[90] L. Blanchet, B. R. Iyer, C. M. Will, and A. G. Wiseman, Class. Quantum Grav. **13**, 575 (1996), gr-qc/9602024.
[91] L. Blanchet, G. Faye, B. R. Iyer, and S. Sinha, Class. Quantum. Grav. **25**, 165003 (2008), 0802.1249.
[92] C. Cutler and E. Flanagan, Phys. Rev. D **49**, 2658 (1994).
[93] K. G. Arun, B. R. Iyer, B. S. Sathyaprakash, and P. A. Sundararajan, Phys. Rev. D **71**, 084008 (2005), erratum-ibid. **D** 72, 069903 (2005), gr-qc/0411146.
[94] R. Balasubramanian, B. S. Sathyaprakash, and S. V. Dhurandhar, Pramana **45**, L463 (1995), gr-qc/9508025.
[95] M. Vallisneri, Phys. Rev. D **77**, 042001 (2008), gr-qc/0703086.
[96] B. Abbott, R. Abbott, T. Abbott, M. Abernathy, K. Ackley, C. Adams, P. Addesso, R. Adhikari, V. Adya, C. Affeldt, et al., Classical and Quantum Gravity **34** (2017), ISSN 0264-9381.
[97] P. Ajith, Phys.Rev. **D84**, 084037 (2011), 1107.1267.
[98] S. Babak, J. Gair, A. Sesana, E. Barausse, C. F. Sopuerta, C. P. L. Berry, E. Berti, P. Amaro-Seoane, A. Petiteau, and A. Klein, ArXiv e-prints (2017), 1703.09722.
[99] R. Fujita, Prog. Theor. Phys. **128**, 971 (2012), 1211.5535.
[100] A. Buonanno and T. Damour, Phys. Rev. D **59**, 084006 (1999), gr-qc/9811091.
[101] J. Veitch et al., Phys. Rev. **D91**, 042003 (2015), 1409.7215.
[102] T. Damour, B. R. Iyer, and B. S. Sathyaprakash, Phys. Rev. D **66**, 027502 (2002), erratum-ibid **66**, 027502 (2002), gr-qc/0207021.